Chemical Science

ROYAL SOCIETY OF CHEMISTRY

EDGE ARTICLE

Check for updates

All publication charges for this article have been paid for by the Royal Society of Chemistry

"Broken-hearted" carbon bowl *via* electron shuttle reaction: energetics and electron coupling†

Gabrielle A. Leith, ‡ Allison M. Rice,‡ Brandon J. Yarbrough, Preecha Kittikhunnatham, Abhijai Mathur, Nicholas A. Morris, Megan J. Francis, Anna A. Berseneva, Poonam Dhull, Richard D. Adams, M. Victoria Bobo, Aaron A. Vannucci, Mark D. Smith, Sophya Garashchuk and Natalia B. Shustova *

Unprecedented one-step C=C bond cleavage leading to opening of the buckybowl (π-bowl), that could provide access to carbon-rich structures with previously inaccessible topologies, is reported; highlighting the possibility to implement drastically different synthetic routes to π-bowls in contrast to conventional ones applied for polycyclic aromatic hydrocarbons. Through theoretical modeling, we evaluated the mechanistic pathways feasible for π-bowl planarization and factors that could affect such a transformation including strain and released energies. Through employment of Marcus theory, optical spectroscopy, and crystallographic analysis, we estimated the possibility of charge transfer and electron coupling between "open" corannulene and a strong electron acceptor such as 7,7,8,8-tetracyanoquinodimethane. Alternative to a one-pot solid-state corannulene "unzipping" route, we reported a nine-step solution-based approach for preparation of novel planar "open" corannulene-based derivatives in which electronic structures and photophysical profiles were estimated through the energies and isosurfaces of the frontier natural transition orbitals.

Introduction

Unzipping nanotubes,[1–5] nanosheets,[6,7] buckyballs,[8–11] or annulenes[12–16] is driven by the renewed interest in fundamental understanding and practical access to novel structural transformations,[17,18] leading to materials with unique optical and electronic profiles. For instance, cutting and unravelling of nanotubes resulted in nanoribbons having electronic properties that can be varied as a function of their width, and therefore, applied in a variety of electronic devices including field-effect transistors, light-emitting diodes, and transparent conductive electrodes.[19,20] In addition, hydrogenation of graphene nanoribbons led to enhanced photoluminescent properties that could pave the way for the development of optically active graphene nanoribbon-based devices.[21] However, promotion of selective C=C bond cleavage in graphitic materials is challenging,[22–24] and although there have been examples of structural changes due to periphery modifications of buckybowls (π-

bowls),[25–28] ring expansion,[22] or opening of the strained π-bowl,[29,30] these accounts are overall very limited. Pursuing the route of C–C bond activation in curved π-bowl-containing systems is advantageous as this could lead to addressing challenges such as selective sphere opening for preparation of endohedral fullerenes, shortening carbon nanotubes (CNTs), guest integration within the CNT body, as well as access to a class of materials that has not been prepared through "wet-chemistry, conventional" routes. One strategy to facilitate C–C bond activation is to employ, for instance, strain energy as a variable, release of which could energetically promote such transformations.[31] Indeed, as presented in this report, release of strain energy can be the driving force for planarization of the naturally curved buckybowl surface (*e.g.*, $C_{20}H_{10}$, corannulene), since there is no direct route to cleave a C=C bond, except through uncontrollable flash vacuum pyrolysis[22,27,29] or addition of a directing group (and a catalyst).[32]

Although there are numerous reports of catalytic hydro-cracking of planar polycyclic aromatic hydrocarbons (PAHs) *i.e.*, increasing the ratio of hydrogen-to-carbon,[33–36] there are very few accounts on C–C bond cleavage following the hydrogenation step.[37] The literature precedent for C–C bond scission primarily relies on the assistance of transition metal catalysts, high hydrogen pressure, elevated temperatures, or a combination of all three parameters.[38–44] Therefore, unexpected C–C bond cleavage (discovered from photophysical studies of alignment of electron donor (corannulene) and acceptor

Department of Chemistry and Biochemistry, University of South Carolina, Columbia, South Carolina 29208, USA. E-mail: shustova@sc.edu

‡ These authors contributed equally.

(7,7,8,8-tetracyanoquinodimethane, TCNQ) in the solid state) reported herein led us to probe mechanistic pathways to determine the feasibility for π-bowl planarization and factors that could affect such a transformation including strain energy (E_s) and released energy (E', Scheme 1, see more details in the ESI†). The electron coupling and charge transfer (CT) rates between "open" corannulene (or parent corannulene) and TCNQ were evaluated by applying Marcus theory. In addition to the solid-state reaction, we also offer more "conventional" solution-based nine-step synthetic routes for the preparation of novel "open" corannulene analogs. In the reported findings, we also discuss the electronic structure and photophysical profiles of the synthesized "open" analogs through estimation of their energies and isosurfaces of the frontier highest occupied and lowest unoccupied natural transition orbitals (HONTO and LUNTO).

Results and discussion

The reductive C=C bond cleavage and consecutive corannulene planarization to form 5,6-dimethyl-benzo[ghi]fluoranthene (planar corannulene analog (P-$C_{20}H_{14}$), Scheme 1) was achieved through a one-pot solid-state reaction, in which corannulene (15 mg, 0.060 mmol), TCNQ (an electron shuttle; 14 mg, 0.068 mmol), and zinc powder (a reducing agent; 50 mg, 0.76 mmol) were ground together (further experimental details can be found in the ESI†). After that, the reaction mixture was placed in a glass tube, a drop of hydrochloric acid (proton source) was added, and the glass tube was flame-sealed under dynamic vacuum (4×10^{-5} mbar). Heating the reaction mixture at 200 °C for six days resulted in the formation of dark brown needle-

shaped crystals suitable for single-crystal X-ray diffraction analysis (Scheme 1). As shown in Scheme 1, such treatment resulted in planarization of the corannulene bowl through partial hydrogenation and formation of P-$C_{20}H_{14}$. X-ray crystallographic studies of $(C_{20}H_{10})\cdot(P\text{-}C_{20}H_{14})\cdot(TCNQ)$ (1) cocrystals revealed that the packing consists of alternating columns of TCNQ and P-$C_{20}H_{14}$ along the c-axis direction (Fig. S1 and S2†). Furthermore, neither mass spectrometry nor spectroscopic studies identified the presence of any other partially hydrogenated products (Fig. S1–S3†).

To gain insight into a plausible mechanism of such π-bowl opening during the one-pot solid-state synthesis (Scheme 1), we initially tested the hypothesis of whether *all* components of the reaction mixture were essential to perform the solid-state C=C bond cleavage. Our results illustrated that the absence of one of the components of the reaction mixture resulted in either no transformation or formation of (corannulene)$_2\cdot$(TCNQ) cocrystals, previously reported in the literature (CCDC 1037414)[45] and also detected in our studies (Fig. S4†). Utilization of a different redox mediator rather than TCNQ (e.g., methyl viologen) did not lead to corannulene opening despite previous reports in which TCNQ and methyl viologen have both been used as electron shuttles in various biological applications.[46–49] Variation of synthetic conditions, for instance, replacement of the zinc powder with sodium dithionite[50] as a reducing agent did not lead to hydrogenated products (see ESI† for more details).

Utilization of more conventional solution-based routes through heating the same reagents ($C_{20}H_{10}$/TCNQ/Zn/HCl) in a series of organic solvents was also attempted. We varied the reaction media starting with the solvents possessing low boiling points (e.g., dichloromethane or methanol), transitioning to dichloromethane/water or methanol/water mixtures, and finally attempting heating in the higher boiling glycerol (b.p. = 290 °C) or ethylene glycol (b.p. = 197 °C) to more closely match the reaction temperature (200 °C) of the solid-state synthesis. In all reactions, no evidence of P-$C_{20}H_{14}$ was detected according to the ^{1}H nuclear magnetic resonance (NMR) spectroscopic or mass spectrometry analysis. Notably, the reported hydrogenation reactions of corannulene typically occurred under relatively harsh conditions (e.g., electron bombardment, alkyllithium reagents, or alkali metals), and even despite them, reactions typically led to hydrogenation of one or two rim C=C bonds without carbon–carbon bond cleavage.[51–57] Since the developed conditions ($C_{20}H_{10}$/TCNQ/Zn/HCl) required the presence of zinc, we also probed the Clemmensen reduction that uses zinc amalgam and concentrated hydrochloric acid.[58] Mass spectrometry and ^{1}H NMR spectroscopy studies of reaction products detected the presence of only pristine corannulene and did not detect any traces of corannulene hydrogenation. As a logical progression, we surveyed an electrochemical method suitable for arene reductive transformations,[59] but proved unsuccessful. Finally, attempts to electrochemically cleave the C=C bond by bulk electrolysis were performed in anhydrous N,N-dimethylformamide or acetonitrile for up to two days, but were also not successful. In line with these studies, we probed the reaction conditions previously utilized for the ring-opening of other
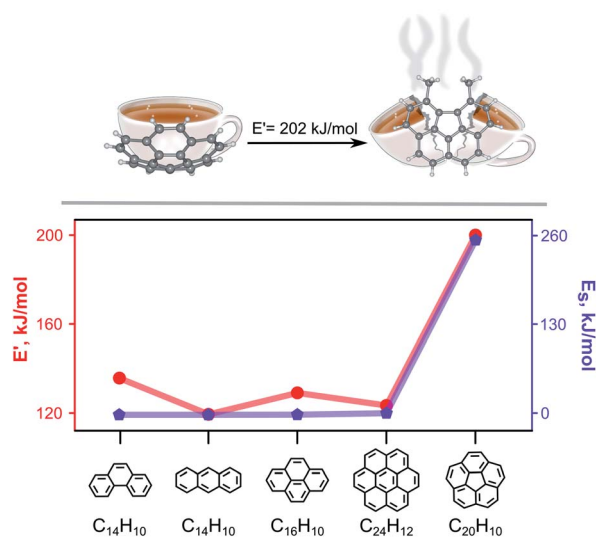
Scheme 1 (*Top*) A schematic representation of π-bowl (corannulene) opening through a solid-state route. Single-crystal X-ray structure of (*left*) corannulene and X-ray structure of (*right*) 5,6-dimethyl-benzo[ghi]fluoranthene (P-$C_{20}H_{14}$) ("open" corannulene). (*Bottom*) Strain energy (E_s, purple)[31] and released energy (E', red) as a function of PAH: (*left to right*) phenanthrene, anthracene, pyrene, coronene, and corannulene.

nonplanar structures such as *o*-carborane.[60–62] For that, we used a triosmium carbonyl complex, $Os_3(CO)_{10}(NCMe)_2$; however, no ring-opening of corannulene was observed, while successful *o*-carborane opening occurred at 150 °C in a nonane reflux.[62]

Further experimental investigations were pursued to rule out aromaticity stabilization as a main factor by performing reactions with significantly less strained PAHs including pyrene (0.0 kJ mol^{-1})[31] or phenanthrene (0.0 kJ mol^{-1})[63] under experimental conditions similar to those used for the reaction with highly-strained corannulene (101 kJ mol^{-1};[31] see ESI† for more details). As a result, no bond cleavage was detected in any of these systems, and formation of only PAH·TCNQ complexes was observed (*e.g.*, phenanthrene·TCNQ complex (similar to the structure reported in the literature[64]) or pyrene·TCNQ complex, Fig. S17; see more details in the ESI†). Thus, this experimental evidence suggests that one of the driving forces for the observed solid-state reaction could potentially be a release of energy through buckybowl planarization (Fig. 2a). To prove this hypothesis, we estimated released energy, E', for PAHs and carbon π-bowls as shown in Scheme 1. For instance, E' for corannulene was calculated to be 202.0 kJ mol^{-1} (Fig. S9, B3LYP/6-31+G*, see the ESI for more details†). In contrast, E' calculated for the PAHs in Scheme 1 was found to be less than 135.7 kJ mol^{-1} (Table S3†). Therefore, corannulene opening is much more energetically favorable in comparison with the PAHs shown in Scheme 1. A similar statement is also valid for a family of extended π-bowls for which the estimated E' was even higher than that of corannulene (Scheme S3†).

The estimated enthalpy of the reaction (eqn (1)),

$$C_{20}H_{10} + 2H_2 = C_{20}H_{14} \tag{1}$$

was found to be −179.5 kJ mol^{-1} (−239 and 59.5 kJ mol^{-1} for only the electronic and the ZPE-corrected electronic energies, respectively, using density functional theory (DFT, Table S2, see the ESI for more details†)). Thus, a combination of two parameters, strain energy (E_s) and released energy (E'), highlights the unique nature of buckybowls in comparison with the considered PAHs (Scheme 1).

As a next step, we took a closer look at a possible mechanism for π-bowl hydrogenation and C–C bond cleavage. On the basis of our theoretical calculations, experimental results, and literature reports, we hypothesized that the transformation of $C_{20}H_{10}$ to P-$C_{20}H_{14}$ occurs in a series of reactions that is first initiated by a sequence of electron and proton transfers in which hydrochloric acid acts as the proton source (Fig. 1). Moreover, probing the strength of the C–C bond revealed a significantly weaker bond (115 kJ mol^{-1} for $C_{20}H_{12}$ and 9 kJ mol^{-1} for $C_{20}H_{12}^{-\bullet}$, Fig. 1) than a typical C–C bond in RCH_2–CH_2R systems, allowing for bond cleavage to occur.[65,66] For instance, if R is a substituent on a pyrene or coronene core then the electronic energy of the C–C bond would be approximately 350 kJ mol^{-1} (Fig. S14†) and 302 kJ mol^{-1}, respectively (Fig. S15†).

Comprehensive analysis of photophysical data for the obtained crystals of **1** revealed properties that are uncharacteristic of the individual components *i.e.*, corannulene and TCNQ themselves. Based on photoluminescence and epifluorescence microscopy studies, the obtained crystals of **1** exhibited red emission (λ_{max} = 705 nm, λ_{ex} = 365 nm) in contrast to their constituents (λ_{max} (TCNQ crystal) = undetectable emission and λ_{max} (corannulene crystal) = 490 nm, λ_{ex} = 365 nm, Fig. S5†). Furthermore, in contrast to diffuse reflectance (DR) profiles of pristine corannulene and TCNQ (Fig. S6†), the appearance of a new red-shifted band (550 nm) in the DR profile of **1** was detected. Based on our theoretical calculations using time-dependent density functional theory (TDDFT), the new band (550 nm) is characteristic of CT complex formation (see the ESI for more details†) that is in line with a previous report on PAHs and TCNQ co-crystals.[24] In particular, according to our studies using the B3LYP-D3/6-311+G** level of theory (Fig. 2b), both
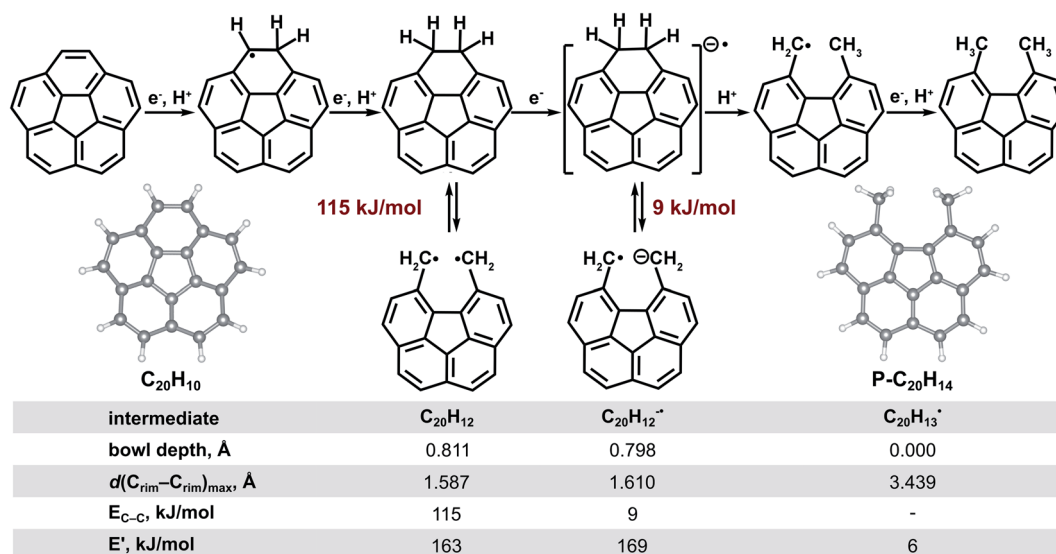

intermediate	$C_{20}H_{12}$	$C_{20}H_{12}^{-\bullet}$	$C_{20}H_{13}^{\bullet}$
bowl depth, Å	0.811	0.798	0.000
$d(C_{rim}–C_{rim})_{max}$, Å	1.587	1.610	3.439
$E_{C–C}$, kJ/mol	115	9	-
E', kJ/mol	163	169	6

Fig. 1 Mechanistic pathway to transform corannulene to P-$C_{20}H_{14}$. Calculations based on B3LYP/6-31+G* level of theory.

a)

a solid-state route

one-pot
Zn/TCNQ
H^+, 200 °C

π-bowl unzipping

X-ray structure of 1

b)

CT

HOMO−2   **TCNQ/P-C$_{20}$H$_{14}$ (1)**   **LUMO**

c)

electron coupling:
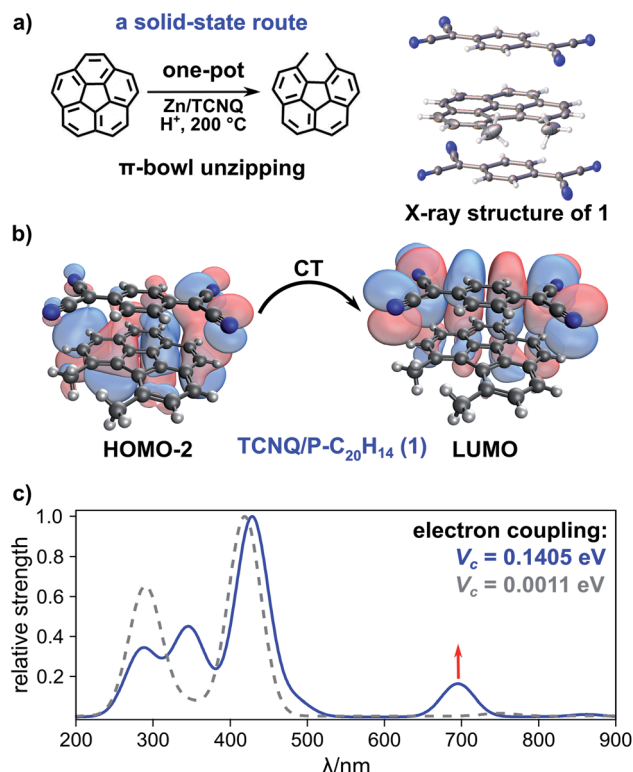V_c = 0.1405 eV
V_c = 0.0011 eV

Fig. 2 (a) (*Left*) Developed route for the preparation of P-C$_{20}$H$_{14}$ and (*right*) a part of the single-crystal X-ray structure of 1 showing an alternating column of TCNQ and P-C$_{20}$H$_{14}$. (b) Molecular orbitals of TCNQ/P-C$_{20}$H$_{14}$ in 1: HOMO−2 and LUMO, related to electron excitation (transition) from P-C$_{20}$H$_{14}$ to TCNQ, respectively. (c) Optical transition strength for TCNQ/P-C$_{20}$H$_{14}$ (blue) and TCNQ/C$_{20}$H$_{10}$ (gray) calculated using TDDFT/RPA based on the B3LYP-D3/6-311+G** level of theory.

a bathochromic shift and new band appearance could be attributed to CT[66,67] between the HOMO−2 and LUMO of a TCNQ/P-C$_{20}$H$_{14}$ "stack" (Fig. 2c). To further shed light on the experimental changes of the emission profile, we examined optical excitations of isolated corannulene, P-C$_{20}$H$_{14}$, TCNQ, and the relevant dimers through the TDDFT calculations based on the B3LYP-D3/6-311+G** method. The considered TCNQ/P-C$_{20}$H$_{14}$ "stack" is the only species with excitation energies of appreciable strength around 690 nm (1.8 eV; Fig. S7†), which is in agreement with the experimentally observed red emission at λ_{max} = 705 nm (Fig. S5†). The lowest excitations for TCNQ, π-bowl, and P-C$_{20}$H$_{14}$ are 413, 288, and 344 nm (3.0, 4.3, and 3.6 eV), respectively (Fig. S7†).

To further probe the idea that CT is more effective in an exclusively planar TCNQ/P-C$_{20}$H$_{14}$ "stack" rather than in a TCNQ/C$_{20}$H$_{10}$ "stack", that encounters steric hindrance from the curved surface of the π-bowl,[45] we employed Marcus theory[68] to compare the electron coupling (that is proportional to CT rate) between TCNQ/C$_{20}$H$_{10}$ and TCNQ/P-C$_{20}$H$_{14}$ using eqn (2):

$$k = 2\pi/\hbar \cdot |V_c|^2 \Big/ \sqrt{(4\pi\lambda k_B T)} \exp\left(-\frac{(\lambda + \Delta G^0)^2}{4\lambda k_B T}\right) \sim |V_c|^2 \quad (2)$$

where k = charge transfer rate, V_c = electron coupling, λ = reorganization energy of the system, and ΔG^0 = energy difference between the initial and final states (see the ESI for more details†). According to the Marcus theory model, TCNQ/P-C$_{20}$H$_{14}$ could result in *ca.* 128-fold increase in electron coupling compared to TCNQ/C$_{20}$H$_{10}$ (Fig. S8 and Table S5, see the ESI for more details†). Since electron coupling is related to the electron transfer rate, we can surmise that there is likely an increased electron transfer rate as well.[66] The charge on the TCNQ molecule was evaluated by applying the Kistenmacher relationship (*i.e.*, correlation between TCNQ intramolecular bond distances and charge on TCNQ)[69] using the crystallographic data of 1 and (corannulene)$_2$·TCNQ co-crystals.[45] In the case of 1, the charge on TCNQ was estimated to be −0.84 and for (corannulene)$_2$-·TCNQ co-crystals was found to be −0.20, suggesting more effective CT can occur in 1 between "open" corannulene (P-C$_{20}$H$_{14}$) and TCNQ. We calculated electronic transitions corresponding to the ground state, first and second excited singlet states of P-C$_{20}$H$_{14}$ in THF (Fig. 3 and S29†). Delocalization of excited energy levels in P-C$_{20}$H$_{14}$ was slightly enhanced, leading to optical transitions of the first and second excited states with values of 399 and 409 nm, respectively (Fig. S29†).

As an alternative scalable approach to access a family of "open" corannulene-containing derivatives, we report a solution-phase route (see ESI†).[70] Despite a number of required steps (Schemes S1 and S2†), in comparison with the one-step solid-state synthesis, the "solution" approach has some advantages since it does not rely on selection of the specific
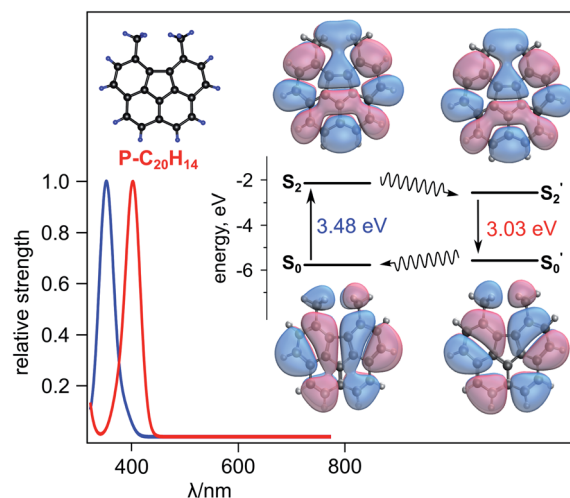

P-C$_{20}$H$_{14}$

S_2

3.48 eV

S_0

S_2'

3.03 eV

S_0'

Fig. 3 (*Top left*) Single-crystal X-ray structure of P-C$_{20}$H$_{14}$. (*Bottom left*) Optical transition strengths computed at the ground state optimal geometry for P-C$_{20}$H$_{14}$ in THF (blue) and at the second excited singlet state optimal geometry for P-C$_{20}$H$_{14}$ in THF (red). (*Right*) Energies and isosurfaces of the HONTO and LUNTO of P-C$_{20}$H$_{14}$ in the ground and the second singlet excited states. S_0 and S_2 are the ground and excited states for P-C$_{20}$H$_{14}$ of the ground state. S_0 and S_2' are the ground and excited state intermediates for the minimum energy geometry of the second excited singlet state. The black solid and wavy arrows indicate absorption ($S_0 \rightarrow S_2$) or emission ($S_2' \rightarrow S_0'$) and vibrational relaxation ($S_2 \rightarrow S_2'$ and $S_2' \rightarrow S_2$), respectively. The theory level is TDDFT/RPA based on the B3LYP-D3/6-31+G* method.

substrate/electron shuttle/reducing agent system and also provides a scalable route for the synthesis of a library of new planar corannulene-type analogs. The synthetic details for

Fig. 4 (a) (*Top left*) Single-crystal X-ray structure of **X**. (*Bottom left*) Optical transition strengths computed at the ground state optimal geometry for **X** in THF (blue) and at the second singlet excited state optimal geometry for **X** in THF (red). (*Right*) Energies and isosurfaces of the HONTO and LUNTO of **X** in the ground and the second singlet excited states. S_0 and S_2 are the ground and excited states for **X** of the ground state. S_0' and S_2' are the ground and excited state intermediates for the minimum energy geometry of the second excited singlet state. The black solid and wavy arrows indicate absorption ($S_0 \rightarrow S_2$) or emission ($S_2' \rightarrow S_0'$) and vibrational relaxation ($S_2 \rightarrow S_2'$ and $S_2' \rightarrow S_2$), respectively. The theory level is TDDFT/RPA based on the B3LYP-D3/6-31+G* method. (b) (*Top left*) Geometrically optimized structure of **X'** based on B3LYP-D3/6-31+G* level of theory. (*Bottom left*) Optical transition strengths computed at the ground state optimal geometry for **X'** in THF (blue) and at the second singlet excited state geometry for **X'** in THF (red). (*Right*) Energies and isosurfaces of HONTO and LUNTO of **X'** in the ground and the second singlet excited states. S_0 and S_2 are the ground and excited states for **X'** of the ground state. S_0' and S_2' are the ground and excited state intermediates for the minimum energy geometry of the second excited singlet state. The black solid and wavy arrows indicate absorption ($S_0 \rightarrow S_2$) or emission ($S_2' \rightarrow S_0'$) and vibrational relaxation ($S_2 \rightarrow S_2'$ and $S_2' \rightarrow S_2$), respectively. The theory level is TDDFT/RPA based on the B3LYP-D3/6-31+G* method.

preparation of 5-methylbenzo[*ghi*]fluoranthene ($C_{19}H_{12}$, **X**, Fig. 4a) and 5-ethyl-6-methylbenzo[*ghi*]fluoranthene ($C_{21}H_{16}$, **X'**, Fig. 4b), using this approach, are provided in ESI.† Sublimation of **X** (Scheme S1†) allowed for the formation of single crystals of **X** suitable for X-ray diffraction (Fig. S24†). The structure of **X'** was confirmed using ^1H and ^{13}C NMR spectroscopy and mass spectrometry (Fig. S21†). As in the case of solid-state "open" P-$C_{20}H_{14}$, both **X** and **X'** structures possess a planar geometry (Fig. S24 and S25†). The emission studies of the prepared **X** and **X'** compounds revealed a red-shifted emission ($\lambda_{max} = 548$ nm and 573 nm, $\lambda_{ex} = 365$ nm, respectively, Fig. S26†) in contrast to pristine corannulene ($\lambda_{max} = 490$ nm, $\lambda_{ex} = 365$ nm, Fig. S5†). The emission maxima of **X** and **X'** in THF was found to be 479 nm and 502 nm, respectively, ($\lambda_{ex} = 365$ nm) and is hypsochromically shifted compared to the solid-state 548 and 573 nm-centered emission, respectively ($\lambda_{ex} = 365$ nm, Fig. 4a, b, S27, and S28†). In a similar vein to TDDFT calculations of P-$C_{20}H_{14}$, we determined the optical transitions corresponding to the ground state, first and second excited singlet states of **X** and **X'** (Fig. S27 and S28†). While the electronic transition of the first excited singlet state for both **X** and **X'** did not differ from the optical transitions corresponding to the ground state (351 nm for **X** and 361 nm for **X'**), optical transitions for the second excited singlet states were determined to be 395 nm and 412 nm for **X** and **X'**, respectively. Electronic transitions corresponding to the second excited singlet state can be associated with the emission profiles that are similar to the experimental data (see the ESI for more details).

Conclusions

To summarize, we report the first example of a unique one-step C=C bond cleavage in the traditionally very robust π-bowl occurring *via* an electron shuttle reaction. Such ring opening is unprecedented in the literature and has not been observed for pristine π-bowls (*e.g.*, corannulene) to date (with the exception of uncontrollable brute force vacuum pyrolysis[22]). PAH hydrogenation has been previously observed under harsh experimental conditions (*e.g.*, high hydrogen pressure or extreme temperatures above 1000 °C),[38–44] therefore the formation of P-$C_{20}H_{14}$ in a one-pot synthesis under relatively mild conditions is an unexpected and remarkable result. Through employment of Marcus theory, optical spectroscopy, and crystallographic analysis, we estimated the electron coupling between "open" corannulene and a strong electron acceptor, TCNQ. A solution-phase route was employed for preparation of two novel "open" corannulene-based derivatives with the corresponding spectroscopic analysis of their properties experimentally and theoretically. Furthermore, through a combination of theoretical modeling with experimental results, mechanistic studies were undertaken to shed light on possible factors (such as strain energy) that could act as a driving force for the observed π-bowl opening. Our studies highlight the possibility to implement novel synthetic routes for π-bowl transformations, that are drastically different from the conventional approaches toward derivatization of traditional PAHs. Thus, the presented solid-state, solution, and theoretical methodology are the first steps
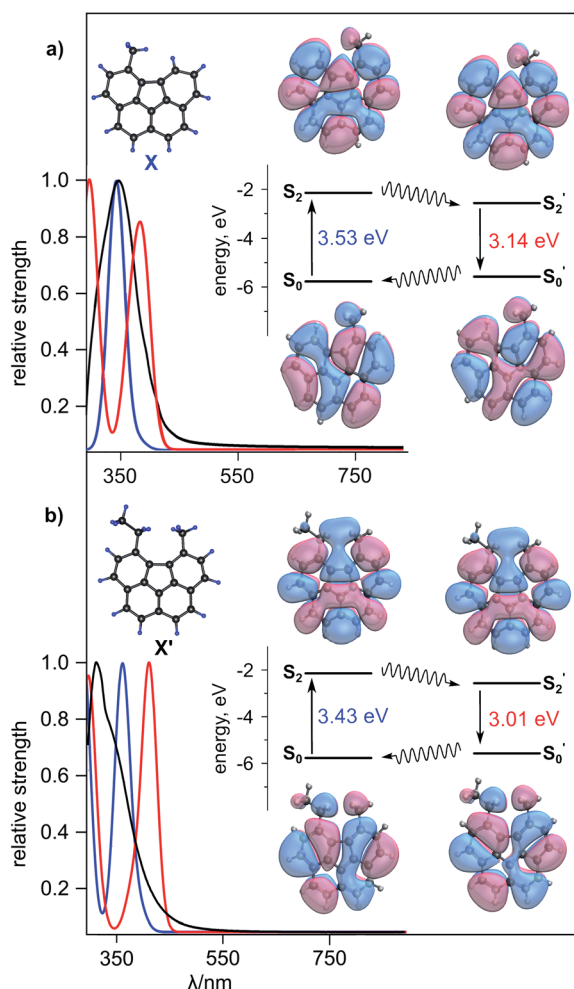
toward understanding possible avenues to prepare barely accessible structures by "unlocking" the corannulene core and application of the latter for molecular electronic development.

Author contributions

Conflicts of interest

There are no conflicts to declare.

Acknowledgements

Notes and references

1 S. V. Rotkin, I. Zharov and K. Hess, *AIP Conf. Proc.*, 2001, **591**, 454–457.

2 V. S. Thoi, R. E. Usiskin and S. M. Haile, *Chem. Sci.*, 2015, **6**, 1570–1577.

3 S.-Y. Zhao, B. Zhang, H. Su, J.-J. Zhang, X.-H. Li, K.-X. Wang, J.-S. Chen, X. Wei and P. Feng, *J. Mater. Chem. A*, 2018, **6**, 4331–4336.

4 M. K. Smith, K. E. Jensen, P. A. Pivak and K. A. Mirica, *Chem. Mater.*, 2016, **28**, 5264–5268.

5 Z. Zhang, Y. Che, R. A. Smaldone, M. Xu, B. R. Bunes, J. S. Moore and L. Zang, *J. Am. Chem. Soc.*, 2010, **132**, 14113–14117.

6 A. Kong, C. Mao, Y. Wang, Q. Lin, X. Bu and P. Feng, *J. Mater. Chem. A*, 2016, **4**, 7305–7312.

7 A. M. Champsaur, J. Yu, X. Roy, D. W. Paley, M. L. Steigerwald, C. Nuckolls and C. M. Bejger, *ACS Cent. Sci.*, 2017, **3**, 1050–1055.

8 G. D. Han, A. Maurano, J. G. Weis, V. Bulović and T. M. Swager, *Org. Electron.*, 2016, **31**, 48–55.

9 O. V. Boltalina, A. A. Popov, I. V. Kuvychko, N. B. Shustova and S. H. Strauss, *Chem. Rev.*, 2015, **115**, 1051–1105.

10 A. Hirsch, *The Chemistry of Fullerenes*, John Wiley and Sons, Inc., 2008.

11 A. M. Rice, E. A. Dolgopolova and N. B. Shustova, *Chem. Mater.*, 2017, **29**, 7054–7061.

12 X. Jiang, S. D. Laffoon, D. Chen, S. Pérez-Estrada, A. S. Danis, J. Rodríguez-López, M. A. Garcia-Garibay, J. Zhu and J. S. Moore, *J. Am. Chem. Soc.*, 2020, **142**, 6493–6498.

13 E. Gonzalez-Rodriguez, M. A. Abdo, G. dos Passos Gomes, S. Ayad, F. D. White, N. P. Tsvetkov, K. Hanson and I. V. Alabugin, *J. Am. Chem. Soc.*, 2020, **142**, 8352–8366.

14 A. V. Zabula, A. S. Filatov, S. N. Spisak, A. Y. Rogachev and M. A. Petrukhina, *Science*, 2011, **333**, 1008–1011.

15 C. Dubceac, A. S. Filatov, A. V. Zabula, A. Y. Rogachev and M. A. Petrukhina, *Chem.–Eur. J.*, 2015, **21**, 14268–14279.

16 Z. Zhou, S. N. Spisak, Q. Xu, A. Y. Rogachev, Z. Wei, M. Marcaccio and M. A. Petrukhina, *Chem.–Eur. J.*, 2018, **24**, 3455–3463.

17 A. Béziau, S. A. Baudron, G. Rogez and M. W. Hosseini, *Inorg. Chem.*, 2015, **54**, 2032–2039.

18 S. A. Baudron and M. W. Hosseini, *Chem. Commun.*, 2016, **52**, 13000–13003.

19 I. Martin-Fernandez, D. Wang and Y. Zhang, *Nano Lett.*, 2012, **12**, 6175–6179.

20 M. Terrones, *ACS Nano*, 2010, **4**, 1775–1781.

21 B. V. Senkovskiy, M. Pfeiffer, S. K. Alavi, A. Bliesener, J. Zhu, S. Michel, A. V. Fedorov, R. German, D. Hertel, D. Haberer, L. Petaccia, F. R. Fischer, K. Meerholz, P. H. M. Van Loosdrecht, K. Lindfors and A. Grüneis, *Nano Lett.*, 2017, **17**, 4029–4037.

22 A. Borchardt, A. Fuchicello, K. V. Kilway, K. K. Baldridge and J. S. Siegel, *J. Am. Chem. Soc.*, 1992, **114**, 1921–1923.

23 Z. Chen, J. A. M. Mercer, X. Zhu, J. A. H. Romaniuk, R. Pfattner, L. Cegelski, T. J. Martinez, N. Z. Burns and Y. Xia, *Science*, 2017, **479**, 475–479.

24 I. V. Alabugin, *Stereoelectronic Effects: A Bridge Between Structure and Reactivity*, John Wiley and Sons, Inc., Hoboken, 2016.

25 Y.-T. Wu and J. S. Siegel, *Chem. Rev.*, 2006, **106**, 4843–4867.

26 B. M. Schmidt, B. Topolinski, M. Yamada, S. Higashibayashi, M. Shionoya, H. Sakurai and D. Lentz, *Chem.–Eur. J.*, 2013, **19**, 13872–13880.

27 L. T. Scott, E. A. Jackson, Q. Zhang, B. D. Steinberg, M. Bancu and B. Li, *J. Am. Chem. Soc.*, 2012, **134**, 107–110.

28 E. Nestoros and M. C. Stuparu, *Chem. Commun.*, 2018, **54**, 6503–6519.

29 S. Attar, D. M. Forkey, M. M. Olmstead and A. L. Balch, *Chem. Commun.*, 1998, 1255–1256.

30 T. Hayama, Y. Wu, A. Linden, K. K. Baldridge and J. S. Siegel, *J. Am. Chem. Soc.*, 2007, **129**, 12612–12613.

31 C. H. Sun, G. Q. Lu and H. M. Cheng, *J. Phys. Chem. B*, 2006, **110**, 4563–4568.

32 S. Tashiro, M. Yamada and M. Shionoya, *Angew. Chem., Int. Ed.*, 2015, **54**, 5351–5354.

33 J. C. Fetzer, *Polycyclic Aromat. Compd.*, 2007, **27**, 143–162.

34 S. Yang and L. M. Stock, *Energy Fuels*, 1996, **10**, 1181–1186.

35 M. A. Nkansah, A. A. Christy and T. Barth, *Polycyclic Aromat. Compd.*, 2012, **32**, 408–422.

36 S. C. Korre, M. T. Klein and R. J. Quann, *Ind. Eng. Chem. Res.*, 1997, **36**, 2041–2050.

37 X.-M. Yue, X.-Y. Wei, S.-Q. Zhang, F.-J. Liu, Z.-M. Zong and X.-Q. Yang, *Fuel Process. Technol.*, 2017, **161**, 283–288.

38 M. Murakami and T. Matsuda, *Chem. Commun.*, 2011, **47**, 1100–1105.

39 R. A. Periana and R. G. Bergman, *J. Am. Chem. Soc.*, 1986, **108**, 7346–7355.

40 C. T. To, K. S. Choi and K. S. Chan, *J. Am. Chem. Soc.*, 2012, **134**, 11388–11391.

41 A. Yamaguchi, N. Mimura, M. Shirai and O. Sato, *Sci. Rep.*, 2017, **7**, 46172.

42 X. Kang, G. Luo, L. Luo, S. Hu, Y. Luo and Z. Hou, *J. Am. Chem. Soc.*, 2016, **138**, 11550–11559.

43 P. Sivaguru, Z. Wang, G. Zanoni and X. Bi, *Chem. Soc. Rev.*, 2019, **48**, 2615–2656.

44 Y. Xia and G. Dong, *Nat. Rev. Chem.*, 2020, **4**, 600–614.

45 Y. Yoshida, K. Isomura, N. Yuto, H. Kishida and G. Saito, *Chem. Lett.*, 2015, **44**, 709–711.

46 M. Wang, C. Wölfer, L. Otrin, I. Ivanov, T. Vidaković-Koch and K. Sundmacher, *Langmuir*, 2018, **34**, 5435–5443.

47 F. P. Van der Zee and F. J. Cervantes, *Biotechnol. Adv.*, 2009, **27**, 256–277.

48 M. D. Peterson, S. C. Jensen, D. J. Weinberg and E. A. Weiss, *ACS Nano*, 2014, **8**, 2826–2837.

49 L. Striepe and T. Baumgartner, *Chem.–Eur. J.*, 2017, **23**, 16924–16940.

50 J. M. Khurana and S. Singh, *J. Indian Chem. Soc.*, 1996, **73**, 487–488.

51 A. Sygula, R. Sygula, F. R. Fronczek and P. W. Rabideau, *J. Org. Chem.*, 2002, **67**, 6487–6492.

52 S. N. Spisak, G. C. Hoover, Z. Wei, A. V. Zabula, A. S. Filatov and M. A. Petrukhina, *Acta Crystallogr., Sect. C: Struct. Chem.*, 2015, **71**, 690–694.

53 E. Shabtai, R. E. Hoffman, P. C. Cheng, E. Bayrd, D. V. Preda, L. T. Scott and M. Rabinovitz, *J. Chem. Soc., Perkin Trans. 2*, 2001, 129–133.

54 R. M. Chin, B. Baird, M. Jarosh, S. Rassman, B. Barry and W. D. Jones, *Organometallics*, 2003, **22**, 4829–4832.

55 R. M. Chin, M. S. Jarosh, J. D. Russell and R. J. Lachicotte, *Organometallics*, 2002, **21**, 2027–2029.

56 P. W. Rabideau, Z. Marcinow, R. Sygula and A. Sygula, *Tetrahedron Lett.*, 1993, **34**, 6351–6354.

57 P. Sundararajan, M. Tsuge, M. Baba, H. Sakurai and Y. P. Lee, *J. Chem. Phys.*, 2019, **151**, 044304.

58 T. Nakabayashi and T. Nakabayashi, *J. Am. Chem. Soc.*, 1960, **82**, 3900–3906.

59 B. K. Peters, K. X. Rodriguez, S. H. Reisberg, S. B. Beil, D. P. Hickey, Y. Kawamata, M. Collins, J. Starr, L. Chen, S. Udyavara, K. Klunder, T. J. Gorey, S. L. Anderson, M. Neurock, S. D. Minteer and P. S. Baran, *Science*, 2019, **363**, 838–845.

60 R. D. Adams, J. Kiprotich, D. V. Peryshkov and Y. Onn, *Chem.–Eur. J.*, 2016, **22**, 6501–6504.

61 R. D. Adams, E. J. Kiprotich and M. D. Smith, *Chem. Commun.*, 2018, **54**, 3464–3467.

62 R. D. Adams, J. Kiprotich, D. V. Peryshkov and Y. O. Wong, *Inorg. Chem.*, 2016, **55**, 8207–8213.

63 Y. Nagano and M. Nakano, *J. Chem. Thermodyn.*, 2003, **35**, 1403–1412.

64 M. A. Dobrowolski, G. Garbarino, M. Mezouar, A. Ciesielski and M. K. Cyrański, *CrystEngComm*, 2014, **16**, 415–429.

65 L. Pauling and L. O. Brockway, *J. Am. Chem. Soc.*, 1937, **59**, 1223–1236.

66 R. J. Dillon and C. J. Bardeen, *J. Phys. Chem. A*, 2012, **116**, 5145–5150.

67 H. N. Ghosh, *J. Phys. Chem. B*, 1999, **103**, 10382–10387.

68 R. A. Marcus, *Rev. Mod. Phys.*, 1993, **65**, 599–610.

69 T. J. Kistenmacher, T. J. Emge, A. N. Bloch and D. O. Cowan, *Acta Crystallogr., Sect. B: Struct. Crystallogr. Cryst. Chem.*, 1982, **38**, 1193–1199.

70 A. M. Butterfield, B. Gilomen and J. S. Siegel, *Org. Process Res. Dev.*, 2012, **16**, 664–676.